NASA Technical Memorandum 107178

Stress and Reliability Analysis of a Metal-Ceramic Dental Crown

Todd M. Sokolowski
The Ohio State University
Columbus, Ohio

Barry Hojjatie
University of Florida
Gainesville, Florida

Noel N. Nemeth
Lewis Research Center
Cleveland, Ohio

Kenneth J. Anusavice
University of Florida
Gainesville, Florida

Prepared for the
ANSYS Conference and Exhibition
sponsored by ANSYS, Inc.
Pittsburgh, Pennsylvania, May 20–22, 1996

National Aeronautics and
Space Administration

STRESS AND RELIABILITY ANALYSIS OF A METAL-CERAMIC DENTAL CROWN

Todd M. Sokolowski
The Ohio State University
Department of Mechanical Engineering
Columbus, Ohio

Barry Hojjatie
University of Florida
College of Dentistry
Gainesville, Florida

Noel N. Nemeth
National Aeronautics and Space Administration
Lewis Research Center
Cleveland, Ohio

Kenneth J. Anusavice
University of Florida
College of Dentistry
Gainesville, Florida

ABSTRACT

Interaction of mechanical and thermal stresses with the flaws and microcracks within the ceramic region of metal-ceramic dental crowns can result in catastrophic or delayed failure of these re-storations. The objective of this study was to determine the combined influence of induced functional stresses and pre-existing flaws and microcracks on the time-dependent probability of failure of a metal-ceramic molar crown. A three-dimensional finite element model of a porcelain-fused-to-metal (PFM) molar crown was developed using the ANSYS® finite element program. The crown consisted of a body porcelain, opaque porcelain, and a metal substrate. The model had a 300 N load applied perpendicular to one cusp, a load of 300N applied at 30 degrees from the perpendicular load case, directed toward the center, and a 600 N vertical load. Ceramic specimens were subjected to a biaxial flexure test and the load-to-failure of each specimen was measured. The results of the finite element stress analysis and the flexure tests were incorporated in the NASA developed CARES/LIFE program to determine the Weibull and fatigue parameters and time-dependent fracture reliability of the PFM crown. CARES/LIFE calculates the time-dependent reliability of monolithic ceramic components subjected to thermomechanical and/or proof test loading. This program is an extension of the CARES (Ceramics Analysis and Reliability Evaluation of Structures) computer program.

NOMENCLATURE

A	surface area; material-environmental fatigue constant
a	crack half length or radius
B	subcritical crack growth constant
$\overline{C}$	Shetty's constant in mixed-mode fracture criterion
g	g-factor
H	step function
I	ranking of ordered fracture data in statistical analysis
K	stress intensity factor
k	crack density coefficient
m	Weibull modulus, or shape parameter
N	material-environmental fatigue constant
n	number of cycles
P	applied force
P_f	cumulative failure probability
Q	cyclic fatigue parameter
R	ratio of minimum to maximum effective stress in a load cycle
T	period of one cycle
t	time or thickness
t_o	time-dependent scale parameter
V	volume; crack velocity
x,y,z	Cartesian coordinate directions
Y	crack geometry factor

α	angle between σ_n and the stress σ_1
β	angle between σ_n projection and the stress σ_2 in plane perpendicular to σ_1
Δ	increment
η	crack density function
π	3.1416
σ	applied stress distribution
σ_o	Weibull scale parameter
$\sigma_1,\sigma_2,\sigma_3$	tensor stress components; principal stresses ($\sigma_1 \geq \sigma_2 \geq \sigma_3$)
τ	shear stress acting on oblique plane whose normal is determined by angles α and β
Ψ	spatial location (x,y,z) and orientation (α,β) in a component
Ω	solid angle in three-dimensional principal stress space for which $\sigma_e \geq \sigma_{cr}$
ω	angle in two-dimensional principal stress space for which $\sigma_e \geq \sigma_{cr}$

Subscripts:

B	Batdorf
c	cyclic; critical
ch	characteristic
cr	critical
d	dynamic fatigue
e,ef	effective
eq	equivalent
f	failure; fracture
I	crack opening mode
II	crack sliding mode
III	crack tearing mode
I	i'th
max	maximum
min	minimum
n	normal; normal stress averaging
S	surface
T	transformed
u	uniaxial
V	volume
w	Weibull
θ	characteristic

Superscripts

~	modified parameter
-	normalized quantity

INTRODUCTION - BRITTLE MATERIAL FAILURE MODES AND DESIGN METHODOLOGY

Ceramics and glasses are two broad classifications of materials that share the same characteristic trait of brittleness. This deficiency represents a concern when stresses must be borne. For instance, ceramics are used for wear parts (nozzles, valves, seals, etc.), cutting tools, grinding wheels, bearings, electronics, human prostheses, and in gasoline and turbine engine environments where the combination of high temperature strength and relative light weight make these materials attractive. Glasses are used, among other things, as containment vessels, including bottles, light bulbs, and television picture tubes, as well as transmission devices such as windows and optical fibers. Among the many requirements for the successful deployment of these components are the proper characterization of material properties and the use of a mature and validated brittle material design methodology.

Ceramics and glasses lack ductility which leads to low strain tolerance, low fracture toughness, and large variations in observed fracture strength. When a load is applied, the absence of significant plastic deformation or microcracking causes large stress concentrations to occur at microscopic flaws, which are unavoidably present as a result of materials processing operations or in-service environmental factors. The observed scatter in component strength is caused by the variable severity of these flaws and by the behavior of sudden catastrophic crack growth which occurs when the crack driving force reaches a critical value. Since ceramics and glasses fail at a critical flaw, examination of their fracture surfaces can reveal the nature of failure. Fractography of broken samples has shown that these flaws can be characterized into two general categories: (1) defects internal or intrinsic to the material volume (volume flaws) and (2) defects extrinsic to the material volume (surface flaws). Intrinsic defects are a result of materials processing. Extrinsic flaws can result from grinding or other finishing operations,chemical reaction with the environment, or the internal defects intersecting the external surface. The different physical nature of these flaws results in dissimilar failure response to identical loading situations.

The ability of a ceramic component to sustain a load may degrade over time. This is caused by a variety of effects such as oxidation, creep, stress corrosion, and cyclic fatigue. Stress corrosion and cyclic fatigue result in a phenomenon called subcritical crack growth (SCG). SCG initiates at an existing flaw and continues until a critical length is reached, causing catastrophic crack propagation. The SCG failure mechanism is a load-induced phenomenon over time. It can also be a function of chemical reaction, environment, debris wedging near the crack tip, and deterioration of bridging ligaments.

Because of the variable severity of inherent flaws, the nature of ceramic failure is probabilistic and optimization of design requires the ability to accurately determine a loaded component's reliability as a function of time in service. Consequently, a successful brittle material design methodology must combine the statistical nature of strength-controlling flaws with fracture mechanics to allow for multiaxial stress states, simultaneously active flaw populations (families of flaws), and subcritical crack growth.

The objective of this paper is to demonstrate this design methodology applied to a dental prosthetic molar crown using the NASA developed integrated design computer program, CARES/LIFE[1,2] (Ceramics Analysis and Reliability Evaluation of Structures LIFE prediction program). With this program, it is possible to identify an optimum geometry and material that will reduce the need for expensive fabrication and testing. The theory and concepts presented in this paper reflect the capabilities of the CARES/LIFE program for time-dependent probabilistic design.

PROGRAM CAPABILITY AND DESCRIPTION

Probabilistic component design involves predicting the probability of failure for a thermomechanically loaded component from specimen rupture data. Typically these experiments are performed with flexural or tensile test specimens of simple geometeries. A static, dynamic, or cyclic load is applied to each specimen until fracture. Statistical strength and SCG (fatigue) parameters are then determined from these data. Using these parameters and the results obtained from finite

element analysis, the time-dependent reliability for a complex component geometry and loading is then predicted. Appropriate design changes are made until an acceptable probability of failure has been reached. This design methodology combines the statistical nature of strength-controlling flaws with the mechanics of crack growth to allow for multiaxial stress states, concurrent (simultaneously occurring) flaw populations, and scaling effects. These issues are addressed within the CARES/LIFE program.

CARES/LIFE predicts the probability of failure of a monolithic ceramic component as a function of service time. It assesses the risk that the component will fracture prematurely as a result of subcritical crack growth. The effect of proof testing components prior to service is also considered. CARES/LIFE is an extension of the CARES[3,4] program. It retains all of the capabilities of the previous CARES code, which include fast-fracture component reliability evaluation and Weibull parameter estimation from inert strength (without SCG contributing to failure) specimen data. CARES/LIFE can estimate parameters that characterize SCG from specimen data as well.

ANSYS® Finite element heat transfer and linear elastic stress analyses are used to determine the component's temperature and stress distributions. The element stress output from ANSYS® is translated into an ASCII character neutral file. The information from the neutral file is then input into CARES/LIFE and the reliability at each element is calculated assuming that randomly distributed volume flaws and/or surface flaws control the failure response. The probability of survival for each element is assumed to be a mutually exclusive event, and the overall component reliability is then the product of all the element survival probabilities. CARES/LIFE describes the probabilistic nature of material strength, using the Weibull cumulative distribution function. The effect of multiaxial stresses on reliability is predicted using the principle of independent action (PIA),[5,6] the Weibull normal stress averaging method (NSA),[7] or the Batdorf theory.[8,9] The Batdorf theory combines the weakest link theory and linear elastic fracture mechanics (LEFM). Conventional fracture mechanics analysis requires that both the size of the critical crack and its orientation relative to the applied loads determine the fracture stress. The Batdorf theory includes the calculation of the combined probability of the critical flaw within a certain size range and located and oriented so that it may cause fracture. A user-selected flaw geometry and a mixed-mode fracture criterion are required to model volume- or surface-strength-limiting defects. Mixed-mode fracture refers to the ability of a crack to grow under the combined actions of a normal load (opening mode) and shear load (sliding and tearing modes) on the crack face. CARES/LIFE includes the total strain energy release rate fracture criterion, which assumes a crack will extend in its own plane (coplanar).[9] Out-of-plane crack extension criteria are approximated by a simple semiempirical equation.[10,11] Available flaw geometries include the Griffith crack, penny-shaped crack, semicircular crack, and notched crack. The Batdorf theory is equivalent to the probabilistic multiaxial theories proposed by Evans[12] and Matsuo.[13]

Subcritical crack growth is difficult to model, because it is a complex phenomenon often involving a combination of failure mechanisms. Existing models usually involve empirically derived crack propagation laws that describe the crack growth in terms of the stress intensity factor at the crack tip plus additional parameters obtained from experimental data.

In CARES/LIFE, the relations describing subcritical crack growth are directly incorporated into the PIA, NSA, and Batdorf theories. Subcritical crack growth is modeled with the power law,[14,15] the Paris law,[16] and the Walker law[17,18] for static and constant-amplitude cyclic loading. These laws use experimentally determined parameters which are material- and environment-sensitive. The power law is used to model stress corrosion cracking in materials such as glasses and alumina exposed to H_2O. Elevated-temperature slow crack growth of silicon nitrides, silicon carbides, and alumina also follows power law behavior.

Some polycrystalline ceramics are prone to strength degradation associated with mechanical damage induced by cyclic loading. The Paris and Walker laws have been suggested as models to account for this behavior.[18] The Walker equation is functionally similar to the Paris equation with additional terms to account for the effect of the R-ratio (minimum cycle stress to maximum cycle stress) on lifetime.

CARES/LIFE is capable of predicting the change in a surviving component's reliability after proof testing is performed. Proof testing is the loading of all components prior to service to eliminate those which may fail prematurely. The components that survive the proof test will have a lower (attenuated) risk of failure in service. In CARES/LIFE the attenuated failure probability is calculated using the PIA, the Weibull normal stress averaging, and the Batdorf theories. The Batdorf model is used to calculate the attenuated failure probability when the proof test load and the service load are not in line or have different multiaxial stress states. This feature is useful when the proof test does not identically simulate the actual service conditions on the component. The durations of the proof test and the service load are also considered in the analysis.

Predicted lifetime reliability of structural ceramic components depends on Weibull and fatigue parameters estimated from widely used tests involving flexural or tensile specimens. CARES/LIFE estimates fatigue parameters from naturally flawed specimens ruptured under static, cyclic, or dynamic (constant stress rate) loading. Fatigue and Weibull parameters are calculated from rupture data of three-point and four-point flexure bars, as well as tensile specimens. For other specimen geometries, a finite element model of the specimen is also required when estimating these parameters.

THEORY

Time-dependent reliability is based on the mode I equivalent stress distribution transformed to its equivalent stress distribution at time t=0. Investigations of mode I crack extension[19] have resulted in the following relationship for the equivalent mode I stress intensity factor

$$K_{Ieq}(\Psi,t) = \sigma_{Ieq}(\Psi,t)\ Y\ \sqrt{a(\Psi,t)} \tag{1}$$

where $\sigma_{Ieq}(\Psi,t)$ is the equivalent mode I stress on the crack, Y is a function of crack geometry, $a(\Psi,t)$ is the appropriate crack length, and Ψ represents a location (x,y,z) within the body and the orientation (α,β) of the crack. In the Weibull and PIA models, Ψ represents a location only. Y is a function of crack geometry; however, herein it is assumed constant with subcritical crack growth. Crack growth as a function of the equivalent mode I stress intensity factor is assumed to follow a power law relationship

$$\frac{da(\Psi,t)}{dt} = A\ K_{Ieq}^{N}(\Psi,t) \tag{2}$$

where A and N are material/environmental constants. The transformation of the equivalent stress distribution at the time of failure, $t=t_f$, to its critical effective stress distribution at time t=0 is expressed as[20,21]

$$\sigma_{Ieq,0}(\Psi,t_f) = \left[\frac{\int_0^{t_f} \sigma_{Ieq}^{N}(\Psi,t)\ dt}{B} + \sigma_{Ieq}^{N-2}(\Psi,t_f) \right]^{\frac{1}{(N-2)}} \tag{3}$$

where

$$B = \frac{2}{A\, Y^2\, K_{Ic}^{N-2}\, (N-2)}$$

is a material/environmental fatigue parameter, K_{Ic} is the critical stress intensity factor, and $\sigma_{leq}(\Psi,t_f)$ is the equivalent stress distribution in the component at time $t=t_f$. The dimensionless fatigue parameter N is independent of fracture criterion. B is adjusted to satisfy the requirement that for a uniaxial stress state, all models produce the same probability of failure. The parameter B has units of stress^2 × time.

Volume Flaw Analysis

The probability of failure for a ceramic component using the Batdorf model[8,9,22] for volume flaws is

$$P_{fV} = 1 - \exp\left\{-\int_V \left[\int_0^{\sigma_{e_{max}}} \frac{\Omega}{4\pi} \frac{d\eta_V(\sigma_{cr})}{d\sigma_{cr}} d\sigma_{cr}\right] dV\right\} \quad (4)$$

where V is the volume, η_V is the crack density function, $\sigma_{e_{max}}$ is the maximum value of $\sigma_{leq,0}$ for all values of Ψ, and Ω is the area of a solid angle projected onto a unit radius sphere in principal stress space containing all crack orientations for which the effective stress is greater than or equal to the critical mode I strength, σ_{cr}. The crack density distribution is a function of the critical effective stress distribution. For volume flaw analysis, the crack density function is expressed as

$$\eta_V(\sigma_{cr}(\Psi)) = k_{BV}\, \sigma_{cr}^{m_V} \quad (5)$$

where k_{BV} and m_V are material constants. The solid angle is expressed as

$$\Omega = \int_0^{2\pi} \int_0^{\pi} H(\sigma_{leq,0},\sigma_{cr}) \sin\alpha\, d\alpha\, d\beta \quad (6)$$

where

$$H(\sigma_{leq,0},\sigma_{cr}) = \begin{cases} 1 & \sigma_{leq,0} \geq \sigma_{cr} \\ 0 & \sigma_{leq,0} < \sigma_{cr} \end{cases}$$

and α and β are the radial and azimuthal angles, respectively, on the unit radius sphere. The transformed equivalent stress $\sigma_{leq,0}$ is dependent on the appropriate fracture criterion, crack shape, and time to failure, t_f. Equation (4) can be simplified by performing the integration of σ_{cr},[22] yielding the time-dependent probability of failure for volume flaw analysis

$$P_{fV}(t_f) = 1 - \exp\left[-\frac{k_{BV}}{2\pi} \int_V \int_0^{2\pi} \int_0^{\frac{\pi}{2}} \sigma_{leq,0}^{m_V}(\Psi,t_f) \sin\alpha\, d\alpha\, d\beta\, dV\right] \quad (7)$$

Fracture criteria and crack shapes available for time-dependent analysis are identical to those used for fast fracture analysis in CARES.[3,4] These fracture criteria include Weibull normal stress averaging (a shear-insensitive case of the Batdorf theory), the total coplanar strain energy release rate, and the noncoplanar crack extension (Shetty) criterion.

For a stressed component, the probability of failure for volume flaw analysis is calculated from equation (7). The finite element method enables discretization of the component into incremental volume elements. CARES/LIFE evaluates the reliability at the Gaussian integration points of the element or, optionally, at the element centroid. Subelement volume is defined as the contribution of the integration point to the element volume in the course of the numerical integration procedure. The volume of each subelement (corresponding to a Gauss integration point) is calculated using shape functions inherent to the element type[4]. Assuming that the probability of survival for each element is a mutually exclusive event, the overall component reliability is then the product of all the calculated element (or subelement) survival probabilities.

Surface Flaw Analysis

The probability of failure for a ceramic component using the Batdorf model[8,9,22] for surface flaws is

$$P_{fS} = 1 - \exp\left\{-\int_A \left[\int_0^{\sigma_{e_{max}}} \frac{\omega}{\pi} \frac{d\eta_S(\sigma_{cr})}{d\sigma_{cr}} d\sigma_{cr}\right] dA\right\} \quad (8)$$

where A is the surface area, η_S is the crack density function, $\sigma_{e_{max}}$ is the maximum value of $\sigma_{leq,0}$ for all values of Ψ, and ω is the arc length of an angle α projected onto a unit radius semi-circle in principal stress space containing all of the crack orientations for which the effective stress is greater than or equal to the critical stress. Analogous to the argument for volume flaws, equation (8) can be reformulated, yielding[22]

$$P_{fS}(t_f) = 1 - \exp\left[-\frac{k_{BS}}{\pi} \int_A \int_0^{\pi} \sigma_{leq,0}^{m_s}(\Psi,t_f)\, d\alpha\, dA\right] \quad (9)$$

The transformed equivalent stress $\sigma_{leq,0}$ is dependent on the appropriate fracture criterion, crack shape, and time to failure, t_f. The fracture criteria and crack shapes available for time-dependent analysis are identical to those used for fast fracture analysis. These fracture criteria include Weibull normal stress averaging (a shear-insensitive case of the Batdorf theory), the total coplanar strain energy release rate, and the noncoplanar crack extension (Shetty) criterion.

The finite element method enables discretization of the surface of the component into incremental area elements. CARES/LIFE evaluates the failure probability at the Gaussian integration points of shell elements or, optionally, at the element centroids. The area of each subelement (corresponding to a Gaussian integration point) is calculated using shape functions inherent to the element type[4]. Assuming that the probability of survival for each element is a mutually exclusive event, the overall component reliability is then the product of all the calculated element (or subelement) survival probabilities.

Static Fatigue

Static fatigue is defined as the application of a nonvarying load over time. For this case the mode I equivalent stress, $\sigma_{leq}(\Psi,t)$, is independent of time and is thus denoted by $\sigma_{leq}(\Psi)$. Integrating equation (3) with respect to time yields

$$\sigma_{leq,0}(\Psi,t_f) = \sigma_{leq}(\Psi) \left[\frac{t_f\, \sigma_{leq}^2(\Psi)}{B} + 1\right]^{\frac{1}{N-2}} \quad (10)$$

Dynamic Fatigue

Dynamic fatigue is defined as the application of a constant stress rate $\dot{\sigma}(\Psi)$ over a period of time, t. Assuming the applied stress is zero at time t=0, then

$$\sigma_{leq}(\Psi,t) = \dot{\sigma}(\Psi)\, t \tag{11}$$

Substituting equation (11) into equation (3) results in an expression for effective stress at the time of failure

$$\sigma_{leq,0}(\Psi) = \left[\frac{\sigma_{leq}^{N}(\Psi,t_f)\, t_f}{(N+1)\, B} + \sigma_{leq}^{N-2}(\Psi,t_f) \right]^{\frac{1}{N-2}} \tag{12}$$

Cyclic Fatigue

Cyclic fatigue is defined as the repeated application of a loading sequence. Analysis of the time-dependent probability of failure for a component subjected to various cyclic boundary load conditions is simplified by transforming that type of loading to an equivalent static load. The conversion satisfies the requirement that both systems will cause the same crack growth.[23] Implicit in this conversion is the validity of equation (2) for describing the crack growth. The probability of failure is obtained with respect to the equivalent static state.

Mencik[23] and Evans[24] defined g-factors, $g(\Psi)$, for various types of cyclic loading, that are used to convert the cyclic load pattern to an equivalent static load. For periodic loading, T is the time interval of one cycle, and $\sigma_{leq}(\Psi)$ is the equivalent static stress acting over the same time interval, t_1, as the applied cyclic stress, $\sigma_{leqc}(\Psi,t)$, at some location Ψ. The equivalent static stress is related to the cyclic stress by

$$\sigma_{leq}^{N}(\Psi)\, t_1 = \int_0^{t_1} \sigma_{leqc}^{N}(\Psi,t)\, dt = t_1 \left[\frac{\int_0^{T} \sigma_{leqc}^{N}(\Psi,t)\, dt}{T} \right] = g(\Psi)\, \sigma_{leqc_{max}}^{N}(\Psi)\, t_1 \tag{13}$$

The CARES/LIFE program uses the maximum cyclic stress, $\sigma_{leqc_{max}}(\Psi)$, of the periodic load as a characteristic value to normalize the g-factor. For a periodic load over a time t_1, the mode I static equivalent stress distribution is

$$\sigma_{leq,0}(\Psi,t_f) = \sigma_{leqc_{max}}(\Psi) \left[\frac{g(\Psi)\, t_f\, \sigma_{leqc_{max}}^{2}(\Psi)}{B} + 1 \right]^{\frac{1}{N-2}} \tag{14}$$

The use of g-factors for determining component life is an unconservative practice for materials prone to cyclic damage. The Walker equation,[17] which has traditionally been used in metals design, has been suggested as a model of fatigue damage for some ceramic materials.[18] The Walker equation describes the crack growth increment per cycle, n, as

$$\frac{da(\Psi,n)}{dn} = A\, K_{Ie_{max}}^{N-Q}(\Psi,n)\, \Delta K_{Ie}^{Q}(\Psi,n) \tag{15}$$

where

$$K_{Ie_{max}}(\Psi,n) = \sigma_{leqc_{max}}(\Psi,n)\, Y \sqrt{a(\Psi,n)}$$

and $\Delta K_{Ie}(\Psi,n)$ represents the range of the stress intensity factor over the load cycle. The subscripts max and min indicate the maximum and minimum cycle stress, respectively. The cyclic fatigue parameters A, N, and Q are experimentally determined. The Walker equation reduces to the Paris law[16] when N and Q are equal in value. The integration of Eq. (15) parallels that of Eq. (2), yielding the cyclic fatigue equivalent stress distribution

$$\sigma_{leqc,0}(\Psi,n_f) = \left[\frac{\int_{n=0}^{n_f} [1-R(\Psi,n)]^{Q}\, \sigma_{leqc_{max}}^{N}(\Psi,n)\, dn}{B} + \sigma_{leqc_{max}}^{N-2}(\Psi,n_f) \right]^{\frac{1}{N-2}} \tag{16}$$

where $R(\Psi,n)$ is the ratio of the minimum to maximum cyclic stress, n_f is the number of cycles to failure, and B is now expressed in units of stress^2 $\times$ cycle. The parameters B and N are determined from cyclic data.

Evaluation of Fatigue Parameters from Inherently Flawed Specimens

Lifetime reliability of structural ceramic components depends on the history of the loading, the component geometry, the distribution of pre-existing flaws, and the parameters that characterize subcritical crack growth. These crack growth parameters must be measured under conditions representative of the service environment. When determining fatigue parameters from rupture data of naturally flawed specimens, the statistical effects of the flaw distribution must be considered along with the strength degradation effects of subcritical crack growth. In the following discussion, fatigue parameter estimation methods are described for surface flaw analysis using the power law formulation for constant stress rate loading (dynamic fatigue). Analogous formulations for volume flaws, static fatigue, and cyclic fatigue have also been developed.[1]

For the uniaxial Weibull distribution the probability of failure is expressed as

$$P_{fs}(t_f) = 1 - \exp\left[-k_{ws} \int_A \sigma_{1,0}^{m_s}(\Psi)\, dA \right] \tag{17}$$

where Ψ represents a location (x,y) and $\sigma_{1,0}$ denotes the transformed uniaxial stress analogous to $\sigma_{leqc,0}$ as defined in equation (13). The Weibull crack density coefficient is given by

$$k_{wS} = \frac{1}{\sigma_{oS}^{m_s}} \tag{18}$$

The Weibull scale parameter, σ_{oS}, corresponds to the stress level where 63.2 percent of specimens with unit area would fail and has units of stress $\times$ area $^{1/m_s}$.

The Weibull parameters are usually determined in an inert environment or at a high enough stressing rate such that crack extension from SCG is negligible. Specimens are usually of simple geometry and loading conditions, such as beams or disks under flexure, or cylindrical specimens under uniform uniaxial tension. The test failure probability can be expressed in terms of the highest stressed point in the specimen, σ_f, using the two-parameter Weibull form

$$P_{fS} = 1 - \exp\left[- A_e \left(\frac{\sigma_f}{\sigma_{oS}} \right)^{m_s} \right] = 1 - \exp\left[- \left(\frac{\sigma_f}{\sigma_\theta} \right)^{m_s} \right] \tag{19}$$

where σ_θ is the characteristic strength of the experimental data and A_e is the effective area. The Weibull modulus and characteristic strength are estimated from specimen rupture data using techniques such as maximum likelihood and least squares as detailed in references 1, 3, and 25. The effective area, A_e, is defined for the uniaxial Weibull distribution as

$$A_e = \int_A \left(\frac{\sigma_1(\Psi)}{\sigma_f} \right)^{m_s} dA \tag{20}$$

where $\sigma_1(\Psi)$ denotes the maximum principal stress distribution. For multiaxially stressed components, the Batdorf technique is used to evaluate the effective area. The analogous formulation for A_e is then

$$A_e = \frac{2\bar{k}_{BS}}{\pi} \int_A \left[\int_0^{\frac{\pi}{2}} \left(\frac{\sigma_{leq}(\Psi)}{\sigma_f} \right)^{m_s} d\alpha \right] dA \tag{21}$$

where the normalized Batdorf crack density coefficient $\bar{k}_{BS} = k_{BS}/k_{wS}$ is used to normalize to the uniaxial stress state. Similar expressions for the effective volume, V_e are determined based on volume flaw formulations.

CARES/LIFE normalizes the various fracture criteria to yield an identical probability of failure for the uniaxial stress state. This is achieved by adjusting the fatigue constant B as well as k_{BS}. For the uniaxial Weibull model this adjusted value is denoted by B_w and for the Batdorf model it is denoted by B_B. From the dynamic fatigue equation (12), substituting B_{wS} for B, N_S for N, the uniaxial stress σ_1 for σ_{leq}, and rearranging equation (17) while assuming that

$$\frac{\sigma_1^2(\Psi,t_f)\, t_f}{(N_S+1)\, B_{wS}} >> 1 \tag{22}$$

the median behavior of the experimental dynamic fatigue data can be described by

$$\sigma_{f_{0.5}} = A_d \dot{\sigma}^{1/(N_S+1)} \tag{23}$$

where $\sigma_{f_{0.5}}$ is the median rupture stress of the specimen and $\dot{\sigma}$ represents the stress rate at the location of maximum stress. The constant A_d is

$$A_d = \left\{ \frac{(N_S + 1)\, B_{wS}\, \sigma_{oS}^{N_S-2}}{\left[\frac{A_{ef}}{\ell n\left(\frac{1}{1-0.50} \right)} \right]^{1/\tilde{m}_s}} \right\}^{1/(N_S+1)} \tag{24}$$

where

$$\tilde{m}_S = \frac{m_S}{N_S - 2}$$

The constants A_d and A_{ef} are obtained by equating risks of rupture. A_{ef} is a modified effective area required for the time-dependent formulation. For the uniaxial Weibull distribution, the expression for the modified effective area is

$$A_{ef} = \int_A \left(\frac{\sigma_1(\Psi,t_f)}{\sigma_f} \right)^{\tilde{m}_s N_s} dA \tag{25}$$

where $\sigma_1(\Psi,t_f)$ denotes the maximum principal stress distribution. For multiaxially stressed components, the Batdorf technique is used to evaluate fatigue parameters. The analogous formulation for A_{ef} is then

$$A_{ef} = \frac{2\bar{k}_{BS}}{\pi} \int_A \left[\int_0^{\frac{\pi}{2}} \left(\frac{\sigma_{leq}(\Psi,t_f)}{\sigma_f} \right)^{\tilde{m}_s N_s} d\alpha \right] dA \tag{26}$$

Equation (24) is applicable except that B_{BS} replaces B_{wS}. The relationship between B_{BS} and B_{wS} for a uniaxial load is established by equating the risk of rupture of the Batdorf model with that of the uniaxial Weibull model[1]

$$\frac{B_{wS}}{B_{BS}} = \left[\frac{\pi \int_A \sigma_1^{\tilde{m}_s N_s}(\Psi,t_f)\, dA}{2\, \bar{k}_{BS} \int_A \int_0^{\frac{\pi}{2}} \sigma_{leq}^{\tilde{m}_s N_s}(\Psi,t_f)\, d\alpha\, dA} \right]^{1/\tilde{m}_s} \tag{27}$$

As N_S becomes large, equation (27) approaches unity.

The terms A_d and N_s in equation (24) are determined from experimental data. Taking the logarithm of equation (23) yields

$$\ell n\ \sigma_{f_{0.5}} = \ell n\ A_d + \frac{1}{N_s + 1}\ \ell n \dot{\sigma} \qquad (28)$$

Linear regression analysis of the experimental data is used to solve equation (28). The median value method is based on least squares linear regression of median data points for various stress rates. Another technique uses least squares linear regression on all the data points. A third option for estimating fatigue parameters is a modification to a method used by Jakus.[26] In this procedure, fatigue parameters are determined by minimizing the median deviation of the logarithm of the failure stress. The median deviation is the mean of the residuals, where the residual is defined as the absolute value of the difference between the logarithm of the failure stress and the logarithm of the median value. In CARES/LIFE this minimization is accomplished by maximizing $\tilde{m}_s$ (N_s + 1)estimated from the data versus the fatigue exponent[1]. CARES/LIFE performs least squares or maximum likelihood Weibull parameter estimation as described by Pai and Gyekenesi[25] to solve for Weibull distribution parameters. The fatigue constant B is obtained from equations (24) and (27).

INTRODUCTION - DENTAL CERAMICS

Recent breakthroughs in materials science and technology have led to improved dental restorative ceramics, metals, and resin-based composites. These breakthroughs have become important since major controversies during this period have centered on allegations of the physiological risks of mercury released from amalgam restorations and environmental concerns regarding waste disposal. In response to this the Swedish government has proposed the progressive elimination of amalgam as a dental restorative material by 1997. Other nations are expected to follow the Swedish model. Among the materials that have been considered as the most biocompatible alternatives to amalgam are dental ceramics. New ceramic products and technologies have gained considerable acceptance in Sweden even though their safety and efficacy have not been fully established.

Ceramic restorations represent one choice for treatment of small to large areas of tooth breakdown in anterior and posterior teeth. Current ceramic products are designed as feldspathic veneering porcelains for a metal substrate (metal-ceramic or porcelain-fused-to-metal restoration) or as components of an all-ceramic restoration. The properties of feldspathic porcelains depend on their composition, microstructure, residual stress state, flaw characteristics, and surface finish. The compositions of dental porcelains for metal-ceramic restorations are often formulated from feldspar and may contain 37-63 wt% SiO_2, 9-17wt% Al_2O_3, 4-15wt% Na_2O, 5-14wt% K_2O, 0-3wt% TiO_2, 0-27wt% ZrO_2, and 4-15wt% SnO_2. Colorant oxides and opacifiers are added for esthetic purposes.

All-ceramic restorations derive their fracture resistance from tougher, higher-strength core ceramics since they lack the high elastic modulus of some metals used as the substructure of metal-ceramic prostheses. Compared with glass ionomer cement and glass-filled resin-based composites that are restricted to lower stress applications, dental ceramics are more durable and less technique sensitive. However, they are more costly and require at least two dental appointments, expect for CAD-CAM restorations that can be machined on-site after an image of the prepared tooth is recorded and transmitted to the computer controlled machining unit. Also, compared with cast-metal or metal-ceramic restorations, all-ceramic restorations are more esthetic, but they are more susceptible to fracture, especially when they are used for reconstruction of molar teeth that are exposed to higher forces. Failure of a ceramic or metal-ceramic restoration may also be caused by debonding, secondary decay at the borders of the restorations, root canal treatment, root fracture, and periodontal disease.

During the past 10 years, advances have been made in the development of ceramics with greater toughness and flexure strength, and of glass-polymer composites with greater wear resistance and higher strength. Although dental ceramics constitute a much more costly alternative than some other materials, they offer the advantages of aesthetics, inertness, durability, low thermal conductivity, and low diffusivity, as compared with amalgams. Compared with resin-based composites, ceramics are not as susceptible to bacterial adhesion and plaque accumulation. While ceramics are generally considered to be inert in the oral cavity, there are certain phenomena associated with their use that may cause significant surface degradation of these materials and subsequent physiological side effects. The survival of these materials as dental restorations depends on their resistance to degradation under the harsh conditions of the oral cavity. These conditions include exposure to a variety of fluids ranging in pH from 2 to 9, thermal cycling between 5 and 55°C, loads of up to 4,345 N as reported by Gibbs et al.[27], attacked by acidulated phoshate fluorides, and abrasion from tooth brushing, professional cleanings, and food substances.

Because of their brittle nature, dental ceramic materials are susceptible to failure from small flaws or cracks under applied tensile stresses. There are several factors which are associated with crack initiation and propagation in dental ceramic restorations, including: (1) shape of the restoration and thickness of ceramic layers; (2) microstructural imhomogene; (3) size and distribution of surface and volume flaws; (4) residual and transient stresses and stress gradients induced by polishing and/or thermal processing; (5) the environment in contact with the restoration (stress corrosion fatigue), (6)repeated loadings (cyclic fatigue from debris wedging at crack tips); (7) thermal expansion or contraction differences; and (8) magnitude and orientation of applied loads. The possible interactions among these variables complicate the interpretation of failure analysis observations.

Fairhurst et al.[28] cite several studies showing that dental porcelains exhibit stress corrosion fatigue. These studies have shown: (1) a lower fracture strength when the porcelain specimens were tested in water as compared to testing in air; and (2) a decrease in breaking strength with increased durations of applied load in water. White[29] showed evidence that feldspathic porcelain undergoes mechanical fatigue as well. Additional research is expected to uncover the role cyclic loading has on the strength of these materials over time. As a consequence, failure over time for dental restorations involves accumulated degradation of the material as well as the occasional instance of overloading and accumulated decay of the tooth at the borders of the restoration. Anusavice[30] has reviewed several clinical studies of porcelain-fused-to-metal (PFM) service lifetime reported by various authors.

Results varied from study to study and a clear consensus regarding lifetime did not emerge. Walton et al. [31] reported a mean life span of 5.7 years and porcelain failure was the second most common failure cause for the bridges and crown surveyed. Maryniuk and Kaplan[32] reported a survey of practicing dentists in which longevity estimates were made for a single-unit PFM restoration and a comparable all gold unit. The PFM units were estimated to have a mean life of 12.7 years versus 14.7 years for the all gold restorations. For a glass-ceramic dental molar crown (Dicor® material), Moffa[33] reported a failure rate of 35% during the first three years. In a similar study Erpenstein and Kerschbaum[34] reported a four-year failure rate of 64%. An earlier study by Linkowski[35] with Cerestore® material indicated a four-year failure rate of 19%.

Fracture surfaces of clinically failed all-ceramic crowns were systematically studied by Thompson et al.[36] for Dicor® and Cerestore® materials. Ten fractured Dicor® and 12 fractured Cerestore® crowns were retrieved and analyzed. The authors conclude that fracture initiation sites appear to be controlled primarily by the location and size of the critical flaw, and not by the specimen thickness. Also, surface preparation and installation technique were important regarding failure mode. All Dicor® crowns displayed fractographic features indicating failure initiation along the internal surface from surface residing flaws as shown in Figure 1, taken from reference 36. The fracture surfaces were relatively smooth and fracture origins were clearly defined. Etching of the surface prior to resin bonding(cementation) introduces a modification of existing flaws. Cerestore® crowns displayed fractographic features indicating failure initiation along the porcelain/core interface, or within the core near the interface. One of the Cerestore® crowns had a failure initiation site on the outer surface of the porcelain layer at the cervical margin; another had a failure initiation site located at a large internal pore within the porcelain layer. Cerestore® fracture surfaces were rough and the core ceramic contained a large volume fraction of porosity. As such, precise location of critical flaws could not be determined. For other types of crowns, the location of failure varies, including localized chipping as a result of Hertzian stresses from contact loads[37].

Kelly et al.[37] investigated all-ceramic fixed partial dentures with the goal of correlating laboratory testing with clinically failed units using finite element analysis and the Weibull distribution function. Anusavice and Hojjatie[38] used finite element analysis to model occlusally loaded glass-ceramic crowns with flaws in the cementatious bonding layer. These are among the first studies attempting to correlate modeling with observed clinical failure modes.

Since it has been demonstrated that ceramic dental restorations fail in a classic brittle manner, brittle material design methodology employing reliability analysis can be useful in the analysis, design and optimization of these restorations. To test this hypothesis this study was designed to demonstrate reliability analysis of a PFM molar crown restoration. Although no clinical study regarding failure analysis of metal-ceramic crowns exists, it is reasonable to expect that the ceramic material behaves in a similar manner as described in the previous studies cited above. A key question to be answered was if the reliability analysis based on an idealized model and finite element analysis could reasonably provide further insight on the failure modes and likely locations of critical flaws in these restorations. Also, the step-by-step process by which testing data is translated into reliability predictions of a dental crown is demonstrated. We speculate that in conjunction with imaging technology (scanning an individual's dental topology), finite element analysis and optimization techniques that employs reliability prediction methodology can lead to improved designs.

EVALUATION OF WEIBULL AND FATIGUE PARAMETERS

To predict the reliability of a component over time in service the material Weibull and fatigue parameters must be known. Weibull and fatigue parameters are obtained from rupture experiments of many nominally identical flawed specimens. In this study reliability is predicted for two materials: (1) Porcelain B (J. F. Jelenko and Co., Armonk, NY, USA) used to form the exposed outer surface of the crown; and (2) Porcelain O (J. F. Jelenko and Co., Armonk, NY, USA) that is applied directly over the surface of the metal layer to reduce visibility of the metal. Both of these materials are feldspathic porcelains. Fast-fracture rupture data for the body 1 (B) and opaque 4 (O) porcelains was obtained from references (39) and (40) respectively. Fatigue rupture experiments were not performed on these materials in reference (39), however dynamic fatigue experiments were performed by Fairhurst et al.[28] on the Porcelain B material. Specific information regarding the experimental setup and testing environment for fast-fracture is described in reference (39). Two specimen configurations were tested; 3-point flexure bars and piston-on-3-ball loaded circular disks. Only the results for the piston-on-3-ball specimens were used herein, since the 3-point data reported in references (39) and (40) suffered from poor dimensional control of the specimen thickness. Additionally, the 3-point specimen inherently can suffer from machining(chip) flaws along the specimen edges (confounding results by introducing a competing failure mode against the natural material flaws). Two major advantages of the piston-on-3-ball configuration is that specimen edges are not highly stressed and that the 3-point fixture can accommodate slightly warped specimens. The disks had an average radius of 8.0 mm, a thickness of 2.0 mm, a support radius of 5.0 mm, and a radius of the load piston of 0.8 mm. Specimen to specimen dimensional variation was negligible.

In order to sample the inert strength distributions, 10 specimens of each material were ruptured in dry air. Note that sample sizes of at least 30 specimens are desired to reduce uncertainty in the accuracy of the estimated parameters (especially the Weibull modulus m). Detailed fractographic examination of the broken samples to determine the identity of flaw populations was not performed. However, fractography is recommended on all specimens. The Weibull plots of the fracture data, Figure 2(a) and (b), and the outlier test in CARES/LIFE did not indicate any strong curvatures or unusual data. This is an indication that the data is unimodal (derived from only one flaw population). Optical examination of the fracture surfaces did not reveal unusual features such as scratch or machining flaws. For this study the flaws are considered to be randomly oriented and distributed exclusively in the material volume (volume flaws) or on the surface (surface flaws). Fracture strengths from references (39) and (40) were determined at the center of the disk (the highest stressed point) at the instant of failure using the formulation recommended by Marshall et al.[41] and Young et al.[42].

$$\sigma_f = \frac{3\,p\,(1+\nu)}{4\,\pi t^2}\left\{1 + 2\,\ln\frac{a}{r_o^*} + \frac{(1-\nu)}{(1+\nu)}\left[1 - \frac{r_o^{*2}}{2\,a^2}\right]\frac{a^2}{R^2}\right\} \qquad (29)$$

$$r_o^* = (1.6r_o^2 + t^2)^{1/2} - 0.675t \quad \text{for} \quad r_o \le t/2$$

$$r_o^* = r_o \quad \text{for} \quad r_o > t/2$$

Where a is the radius of the balls from the center of the disk, r_o is the radius of the piston, R is the radius of the disk, t is the thickness of the disk, and P is the applied force. Figure 2(a) and (b) show a Weibull plot of the fracture stresses. The Porcelain O is significantly stronger than the Porcelain B. Note this figure also includes Kanofsky-Srinivasan 90% confidence bands[25]. As indicated in reference (39), equation (29) correlates well with results from 3-dimensional finite element analysis when disk dimensions and load spacings are within certain ranges. However, for parameter estimation purposes the effective volume and area (see equations (20) and (21)) must additionally be computed. Consequently the stress distribution throughout the disk must be known. Because of the loading complexity and presence of multiaxial stress states, the integration is performed numerically in CARES/LIFE using the results from ANSYS® finite element analysis. A one-third finite element model of the piston-on-3-ball disk was used to study the specimen's stress distribution. The specimen disk model consists of solid elements (ANSYS® element SOLID45) and shell elements (ANSYS® element SHELL63) where mesh density is highest at the disk center on the tensile surface. A sufficiently refined mesh is essential for reliability analysis since stresses are exponentiated by the Weibull modulus in the stress-volume (-area) integral. Hence, the accuracy of results is highly sensitive to the accuracy of the stress solution. The solid elements are used for the volume flaw formulations. Shell elements were placed on the surface of the model sharing common nodes with the solid elements. The shell elements were set with a very small (1×10^{-6} mm) thickness and with membrane properties only (no bending stiffness) so that a negligible amount of stiffness was added to the problem. The presence of the shell elements yielded the in-plane elemental surface stresses and corresponding elemental areas. Figure 3 is a first-principal-stress plot for the specimen disk. Stresses predicted by FEA were consistently within a few percent of the closed form approximation (equation (29)).

The effective volume, V_e, and area, A_e, were calculated with CARES/LIFE using the Batdorf methodology (see equation (21)), Shetty's mixed-mode fracture criterion[11], and a penny-shaped crack for the volume flaw and a semi-circular crack for the surface flaw (further details are given in refs. 1 and 3). Table 1 summarizes the results from CARES/LIFE of the Weibull modulii, characteristic strengths, effective volumes and areas, as well as the scale parameters for the two materials (as described by equations (18) to (21)). These parameters are used for the subsequent fast-fracture reliability analysis.

Assuming that small crack-like imperfections control the failure, the material strength in multiaxial stress states can be correlated to the effects of mixed-mode loading on the individual cracks.[8,9] Shetty[11] developed a simple equation describing the ability of a crack to extend under the combined actions of a normal and shear load on the crack face using an empirically determined parameter, $\bar{C}$. For a semicircular crack this equation is[3]

$$\sigma_{1eq} = \frac{1}{2}\left[\sigma_n + \sqrt{\sigma_n^2 + 3.301\left(\frac{\tau}{\bar{C}}\right)^2}\right] \qquad (30)$$

where σ_n and τ are the normal and shear stresses, respectively, acting on the flaw plane. For a penny-shaped crack this relationship is

$$\sigma_{1eq} = \frac{1}{2}\left[\sigma_n + \sqrt{\sigma_n^2 + \left(\frac{4\,\tau}{\bar{C}\,(2-\nu)}\right)^2}\right] \qquad (31)$$

A value of $\bar{C} = 0.82$ approximates the non-coplanar strain energy release rate criterion.

The dynamic fatigue specimen rupture data from Fairhurst et al.[28] was used to obtain fatigue parameters for Jelenko Gingival por-celain B. Fairhurst et al.[28] also determines fatigue parameters for a second material, designated C1/C3 Model porcelain. The parameters, for the C1/C3 Model material, are used for the porcelain O in this study (for the time-dependent reliability analysis). Note porcelain C1/C3 Model and porcelain O have similar Weibull parameters as shown in Table 1 and Table 2. We conjecture that the two porcelains (C1/C3 Model and O) will generally have a similar fatigue behavior because of the similarity of the glass components of the two materials. The C1/C3 Model is a bimaterial consisting of a high leucite-containing component (C1), and the glass component (C3), provided by Jelenko Dental Health Products, Armonk, NY. A mixture of 0.6 C1 and 0.4 C3 was used for the model system. Beam deflection of specimens from this composition matched the beam deflection of the body porcelain (indicating the Young's modulus of C1/C3 Model is similar to the value for the porcelain O). Further information regarding the material compositions and experimental setup and testing environment is described in reference 28.

Again a piston-on-3-ball specimen configuration was used, except with a disk radius of 6.00 mm, a thickness of 1.00 mm, a support radius of 3.16 mm, and a piston radius of 0.78 mm. Equation (29) was used to determine peak fracture stresses[43] and a finite element model of the specimen was prepared. Each material was tested at five stressing rates (100, 10, 1, 0.1, and 0.01 MPa/s) in water (to simulate the oral environment), and also in a dry (inert) environment. All tests were performed at 37° C. Fifty B and twenty C1/C3 Model porcelain specimens were tested at each stressing rate. One hundred B and twenty C1/C3 porcelain specimens were tested in fast-fracture. Individual specimen fracture stresses were not available[43], however reference (28) gives median rupture stress values at each stressing rate, as reproduced in Figure 4(a) and (b). Figure 4 also shows median regression line and the 90% prediction band of the scatter in the data estimated from CARES/LIFE. Fortunately, the data reported

by Fairhurst et al.[28] are sufficient to utilize the parameter estimation capabilities of CARES/LIFE (see equations (28), (26), (24), (21), and (19)). Using these results and finite element analyses of the specimen, the Weibull and fatigue parameters were calculated and listed in Table 2. The values listed in Table 2 were calculated based on specific specimen geometry, loading, crack shapes, and the fracture criterion; hence, the results are not directly comparable to reference 28 (which did not consider these factors). Also, the difference in the fatigue exponent N from this study and that of Fairhurst et al.[28] is associated with regression being performed on median values versus regression performed on all fracture stresses.

RELIABILITY ANALYSIS OF A PFM MOLAR CROWN

The ANSYS® Revision 5.1 FEA program was used to create the model of the ceramic-metal dental restoration and analyze various load cases. Although a molar crown can be analyzed by an axisymmetric model [38,44], a three-dimensional model needed to be created[45] to analyze stresses in the crown subjected to a nonsymmeteric loading condition. A three-dimensional finite element model of a mandibular second molar crown was developed and the overall dimensions were selected to be consistent with the values identified by Wheeler[46] for an average molar crown. It was assumed that the natural enamel in the prepared areas was completely removed.

The model of one half of the PFM crown is composed of four materials. Figure 5 is a cross-sectional view of the this 3-dimensional model. At the center is the pulp chamber (modeled as a void). The dentin layer is the remaining part of the original tooth, to which the restoration is affixed. Directly in contact with the dentin is a thin layer of metal, since the cement layer was ignored with this model. A 200 μm nickel-chromium alloy coping acts as a support to alleviate stress build-up within the ceramic. The metal layer is covered by two layers of ceramic materials. The outer ceramic is porcelain B (J.F. Jelenko and Co., Armonk, N.Y.) and the inner ceramic is known as porcelain O (J.F. Jelenko and Co., Armonk, N.Y.). We have assumed that residual stresses (which are induced in the ceramic due to contraction differences between the metal, Opaque 4,and Porcelain B layers and nonuniform distribution of temperature during high aspect processing) were negligible. Failure or debonding in the metal layer was not investigated (perfect bonding was assumed). A cement layer, which is used to bond the metal to the dentin was not considered. The materials were assumed to be homogeneous, linearly elastic, and isotropic.

The model is composed of 9504 volume elements and 1685 surface elements. The volume elements are ANSYS® SOLID45 3-D structural solid 8 node brick elements, all of which are full bricks (none are collapsed to prisms or tetrahedrons). The surface elements are ANSYS® SHELL63 elastic shell elements which are all collapsed to three-node triangles. Mesh density was concentrated in areas of high stress so accuracy could be maintained. The elastic modulus values for porcelain B, porcelain O, Ni-Cr alloy, and the dentin were 68.0, 75.0, 210.0, and 18.6 GPa, respectively, and the corresponding Poisson's ratios were 0.28, 0.28, 0.33, and 0.31, respectively. The effect of the pulp region on stress was considered to be negligible. General guidelines for material thickness were followed such that the body porcelain thickness was generally 1.05 mm thick, the opaque porcelain was 0.35 mm thick, and the Ni-Cr alloy was held constant at a thickness of 0.20 mm. The overall height of the tooth-crown combination was 9.1 mm, and the width at the root was 6.00 mm. The use of a three-dimensional model allowed concentrated directional loading on one cusp of the crown to be examined (rotational or twisting loads were not considered). A simple fixed support is assumed at the bottom (root) portion of the dentin and the plane of symmetry is fixed with respect to out of plane displacements and rotations. The top surface of the crown had gradual height undulations varying by 0.50 mm to simulate the four cusps.

To study surface stresses, shell elements were placed on selected surfaces sharing common nodes with the solid elements. The outer surface of porcelain B had shell elements placed on the areas surrounding the load and the opposing side of the restoration. The areas which are shared by the metal layer and porcelain O also had shell elements applied to them. These surfaces were expected to experience the highest stresses for the various load cases investigated. The interface between the two porcelain materials was not examined since they have similar elastic modulus. The shell elements were set with a very small thickness ($1x10^{-5}$ mm) and with membrane properties only (no bending stiffness) so that a negligible amount of stiffness was added to the problem. Note that the capability to selectively add shell elements enabled interior surfaces to be analyzed and planes of symmetry to be ignored (not erroneously recognized as a surface). The presence of the shell elements yielded the in-plane elemental surface stresses and corresponding elemental areas.

Two-dimensional finite element stress analysis of ceramic crowns for anterior teeth indicate that the loading orientation is a major cause of tensile stresses[40]. As a result three loading cases were used to evaluate the stress distribution within the restoration. The first case was a load of 300 N applied perpendicular to the face of one cusp. The second load case was a 300 N load applied 30 degrees from perpendicular directed toward the center of the tooth. The third load case was a 600 N load applied vertically at the peak of the cusp. The loads were distributed over the surface of 10 elements which made up an area of roughly $0.5mm^2$ (one square millimeter for a whole 360 degree restoration). Direct forces were applied to the nodes of these elements. All three load cases were investigated for fast-fracture reliability. The first load case was also investigated for cyclic loading by assuming it approximated a chewing action.

Figure 6 shows first-principal stress plots for the three load cases. All the load cases indicate highest stresses are in the metallic layer. Maximum stress within the metal layer was 73 MPa, which is well below the 690 MPa yield strength of the alloy. As shown in the plots, the high elastic modulus of the metal alleviates stress build-up in the porcelain materials, especially at the opaque-metal boundary. In fact stresses in the opaque porcelain near the metal layer, although tensile, are quite low in magnitude (maximum stress was 26 MPa). Certainly, debonding and metal fatigue resulting in stress redistribution and allowing the oral environment to contact with the opaque porcelain can drastically affect the integrity of the restoration, but these failure modes were not considered. Peak stress for the porcelains consistently occur in the porcelain B surrounding the load. This is an expected result of the Hertzian type of loading. Obviously other loading distributions may reduce or increase this localized stress. For the loading situations used in this study the Hertzian

stress are believed to be realistic and capable of inducing material damage. Whether this damage would remain as localized cracking, chipping, or result in failure of the restoration is beyond the scope of this study. Suffice it to say that even localized cracking or chipping could necessitate repair or replacement of the crown, and therefore is an undesirable situation we consider equivalent to a "failure." Overall, while the highest porcelain stresses occur on the porcelain B surfaces, there is also a significant distribution of tensile stress throughout both porcelain volumes. This situation is significant regarding the reliability of the restoration.

The degree of crack growth is dependent on both the magnitude and the duration of the applied stress. Therefore, it is not only difficult to estimate the effective applied stress in the oral environment, but the life estimation may be further complicated by crack healing or blunting of the crack tip during prolonged non-stress periods. This analysis is based on conservative assumptions regarding the statistics and physics of crack growth. Thus, predicted lifetimes will represent lower bounds with respect to material integrity. Of course, unaccounted failure modes will change lifetime estimations and this analysis did not consider the integrity of the bonding. Keeping this caveat in mind, reliability results for the three loading cases can be discussed. Fractography of specimen surfaces were not segregated into flaw type, which would allow concurrent flaw populations to be considered in the reliability analysis. Reliability results are presented based either on volume flaw failures or surface flaw failures, but not both simultaneously. Figure 7 shows a Weibull plot of the overall results for the fast-fracture probability of failure versus the magnitude of applied loading for the molar crown for volume flaw analysis. The crown is much more sensitive to flaws distributed in the volume than flaws residing on the surface. This is a reasonable result, since the volume under tensile load is much greater in the crown than the flexure specimen disks. In contrast to this, the area fraction of the crown that experiences tensile stress relative to that of the disk specimen is significantly smaller. This does not mean that the crown will fail from volume flaws and not surface flaws. Rather it points to the need to firmly establish the identity of flaws in the disk specimen experiments. Also, since flexure tests are especially sensitive to surface flaws, these results perhaps point to the need for further tensile specimen testing where more of the specimen volume can be exposed to high levels of stress. Table 3 is a breakdown of the failure probability for each material under the three load cases for surface and volume flaw analysis. The material numbers represent various slices from the whole model geometry. It is clear that the porcelain B is driving the failure response and not the porcelain O. This is understandable, since the porcelain B is a weaker material than the porcelain O (they both have similar Weibull moduli) and the highest stresses are experienced by the body porcelain, especially as a result of Hertzian contact stresses. Obviously, Hertzian stresses are strongly dependent on the nature of the load, placement of the load, and the topology of the crown surface. Consequently one must be careful when extrapolating these results in a general fashion to clinical experiences. On the other hand, stresses around the metal layer seem less sensitive to the loading. Therefore, meaningful design guidelines may be more feasible here. Obviously, a clinical and laboratory study further exploring these issues is needed here before firm conclusions can be reached.

The time-dependent probability of failure is shown in Figure 8. This was for surface flaws on the exposed areas of the porcelain B. It was assumed that the interior surfaces of the porcelains at the metallic layer and at the interface of the two porcelains were not exposed directly to the environment. Further it was assumed that the volume flaws were not exposed to the oral environment. Of course, depending on porosity or the ability of the saliva to diffuse into the material this may or may not be a correct assumption. However, without a firm basis to assume stress corrosion can occur inside the material, the issue is ignored here. Since dental porcelains are sensitive to mechanical fatigue effects[29] a volume and surface flaw analysis investigating ramifications of material integrity using the Walker law (detailed in equations (15) and (16)) is desireable. Unfortunately, the current lack of usable data regarding this phenomenon precludes presenting results here. Based on the stress corrosion data from Fairhurst et al.[28] we are assuming a cyclically applied sawtooth loading waveform with a stress ratio of zero (R=0.0). Assuming a cyclic frequency of 1 Hertz allows reliability to be predicted as a function of the number of cycles. For the various constant peak applied loads indicated in the figure, the effect of stress cycles on reliability is revealed.

CONCLUSION

The use of ceramics for load-bearing applications depends on the strength, toughness, and reliability of these materials. Ceramic components can be designed for long service life if the factors that cause material failure are considered. This design methodology must combine the statistical nature of strength controlling flaws with fracture mechanics to allow for multiaxial stress states, concurrent flaw populations, and subcritical crack growth. This has been accomplished with the CARES/LIFE public domain computer program for predicting the time-dependent reliability of monolithic structural ceramic components. CARES/LIFE has been used in this study to examine the durability of a ceramic-metal molar dental restoration.

For all load cases, fast-fracture failure occurred in the porcelain B volume. One of the reasons for this was the stress distribution within that volume. Results of this analysis have shown that the nickel-chromium coping successfully relieves stress from the ceramic components of the PFM restoration by absorbing the high stresses. The maximum stress in the metal layer was 73 MPa, which is well under the 690 MPa yield strength[47] of the metal. Since the stresses are relatively low in the region of porcelain O and they are relatively insensitive to surface topology, failure of the restoration is not likely to occur here. However, if debonding or metal fatigue was to occur because of the high stress in the metal, the chance for failure in the porcelain O would likely be much higher.

The combination of a concentrated load, stress distribution, and volume flaws control the probability of failure within the volume of the restoration. The concentrated load produced a Hertzian stress distribution. The load most likely to initiate failure was oriented 30 degrees from perpendicular, which produced very high tensile stresses on the tip of the loaded cusp. Porcelain B sustained the highest stresses and therefore the greatest probability of failure.

FUTURE WORK...

Future work should contrast the results in this paper for a PFM crown versus an all-ceramic crown luted with cement. The influence of reduced metal thickness on the reliability of PFM crowns is also being studied. Ultrathin metal thickness of 0.1 mm has been proposed for use with PFM restorations, but the long-term durability of these crowns has not been fully investigated.

REFERENCES

1. Nemeth, N.N., Powers, L.M., Janosik, L.A., and Gyekenyesi, J.P., "Ceramics Analysis and Reliability Evaluation of Structures LIFE prediction program (CARES/LIFE) Users and Programmers Manual," TM-106316, to be published.
2. Nemeth, N.N., Powers, L.M., Janosik, L.A., and Gyekenyesi, J.P., "Time-Dependent Reliability Analysis of Monolithic Ceramic Components Using the CARES/LIFE Integrated Design Program," Life Prediction Methodologies and Data for Ceramic Materials, ASTM STP 1201, C.R. Brinkman, and S.F. Duffy, Eds., American Society for Testing and Materials, Philadelphia, 1993.
3. Nemeth, N.N., Manderscheid, J.M., Gyekenyesi, J.P., "Ceramics Analysis and Reliability Evaluation of Structures (CARES)," NASA TP-2916, Aug. 1990.
4. Powers, L.M., Starlinger, A., Gyekenyesi, J.P., "Ceramic Component Reliability With the Restructured NASA/CARES Computer Program," NASA TM-105856, Sept. 1992.
5. Barnett, R.L., Connors, C.L., Hermann, P.C., and Wingfield, J.R., "Fracture of Brittle Materials Under Transient Mechanical and Thermal Loading," U.S. Air Force Flight Dynamics Laboratory, AFFDL-TR-66-220, 1967. (NTIS AD-649978)
6. Freudenthal, A.M., "Statistical Approach to Brittle Fracture," Fracture, Vol. 2: An Advanced Treatise, Mathematical Fundamentals, H. Liebowitz, ed., Academic Press, 1968, pp. 591-619.
7. Weibull, W.A., "The Phenomenon of Rupture in Solids," Ingenoirs Vetenskaps Akadanien Handlinger, 1939, No. 153.
8. Batdorf, S.B. and Crose, J.G., "A Statistical Theory for the Fracture of Brittle Structures Subjected to Nonuniform Polyaxial Stresses," Journal of Applied Mechanics, Vol. 41, No. 2, June 1974, pp. 459-464.
9. Batdorf, S.B., and Heinisch, H.L., Jr., Weakest Link Theory Reformulated for Arbitrary Fracture Criterion. Journal of the American Ceramic Society, Vol. 61, No. 7-8, July-Aug. 1978, pp. 355-358.
10. Palaniswamy, K., and Knauss, W.G., On the Problem of Crack Extension in Brittle Solids Under General Loading, Mechanics Today, Vol. 4, 1978, pp. 87-148.
11. Shetty, D.K., Mixed-Mode Fracture Criteria for Reliability Analysis and Design with Structural Ceramics. Journal of Engineering for Gas Turbines and Power, Vol. 109, No. 3, July 1987, pp. 282-289.
12. Evans, A.G., "A General Approach for the Statistical Analysis of Multiaxial Fracture," Journal of the American Ceramic Society, Vol. 61, 1978, pp 302-306.
13. Matsuo, Y., Trans. of the Japan Society of Mechanical Engineers, Vol. 46, 1980, pp. 605-611.
14. Evans, A.G., and Wiederhorn, S.M., "Crack Propagation and Failure Prediction in Silicon Nitride at Elevated Temperatures," Journal of Material Science, Vol. 9, 1974, pp. 270-278.
15. Wiederhorn, S.M., Fracture Mechanics of Ceramics. Bradt, R.C., Hasselman, D.P., and Lange, F.F., eds., Plenum, New York, 1974, pp. 613-646.
16. Paris, P., and Erdogan, F., "A Critical Analysis of Crack Propagation Laws," Journal of Basic Engineering, Vol. 85, 1963, pp. 528-534.
17. Walker, K., "The Effect of Stress Ratio During Crack Propagation and Fatigue for 2024-T3 and 7075-T6 Aluminum," ASTM STP 462, 1970, pp. 1-14.
18. Dauskardt, R.H., James, M.R., Porter, J.R., and Ritchie, R.O., "Cyclic Fatigue Crack Growth in SiC-Whisker-Reinforced Alumina Ceramic Composite: Long and Small Crack Behavior," Journal of the American Ceramic Society, Vol. 75, No. 4, 1992, pp. 759-771.
19. Paris, P.C., and Sih, G.C., Stress Analysis of Cracks. ASTM STP 381, 1965, pp. 30-83.
20. Thiemeier, T., "Lebensdauervorhersage fun Keramische Bauteile Unter Mehrachsiger Beanspruchung," Ph.D. dissertation, University of Karlesruhe, Germany, 1989.
21. Sturmer, G., Schulz, A., and Wittig, S., "Lifetime Prediction for Ceramic Gas Turbine Components," ASME Preprint 91-GT-96, June 3-6, 1991.
22. Batdorf, S.B., "Fundamentals of the Statistical Theory of Fracture," Fracture Mechanics of Ceramics, Vol. 3, eds., Bradt, R.C., Hasselman, D.P.H. and Lange, F.F., Plenum Press, New York (1978), pp. 1-30.
23. Mencik, J., "Rationalized Load and Lifetime of Brittle Materials," Communications of the American Ceramic Society, Mar. 1984, pp. C37-C40.
24. Evans, A.G., "Fatigue in Ceramics," International Journal of Fracture, Dec. 1980, pp. 485-498.
25. Pai, S.S., and Gyekenyesi, J.P., Calculation of the Weibull Strength Parameters and Batdorf Flaw Density Constants for Volume and Surface-Flaw-Induced Fracture in Ceramics, NASA TM-100890, 1988.
26. Jakus, K., Coyne, D.C., and Ritter, J.E., "Analysis of Fatigue Data for Lifetime Predictions for Ceramic Materials," Journal of Material Science, Vol. 13, 1978, pp. 2071-2080.
27. Gibbs,C.H., Mahan,P.E., Mauderli, A., Lundeen,H.C.and Walsh, E. K. "Limits of human bite strength," J. Prosthet. Dent. (1986) 56(2), 226-230.
28. Fairhurst, C.W., Lockwood, P.E., Ringle, R.D., and Twiggs, S.W., "Dynamic Fatigue of Feldspathic Porcelain," Dental Materials, Vol. 9, July, 1993, pp. 269-273.
29. White, S.N., "Mechanical Fatigue of a Feldspathic Dental Porcelain," Dental Materials, Vol. 9, July, 1993, pp. 260-264.
30. Anusavice, K.J., "Quality Evaluation of Dental Restorations: Criteria for Placement and Replacement of Dental Restorations: Oct. 19-21, 1987, Lake Buena Vista, FL., Anusavice, K.J., editor; Quintessence, Chicago, 1989, pp. 15-56.
31. Walton, J.N., Gardner, F.M., and Agar, J.R., "A Survey of Crown and Fixed Partial Denture Failures: Length of Service and Reasons for Replacement," Journal of Prosthetic Dentistry, Vol. 56, 1986, pp. 416-421.
32. Maryniuk, G.A., and Kaplan, "Longevity of Restorations: Survey results of Dentists' Estimates and Attitudes," Journal of the American Dental Association, Vol. 112, 1986, pp. 39-45.

33. Moffa, J.P., "Clinical Evaluation of Dental Restorative Materials Final Report," Interagency Agreement No. 1Yo1PDE40001 P05, Letterman Army Institute of Research, San Francicso, 1988.
34. Erpenstein, H., and Kerschbaum, T., "Frakturrate von Dicor'-Kronen Unter Klinischen Bedingungen," Dtsch Zahndrztl Z, Vol. 46, 1991, pp. 124-128.
35. Linkowski, G., "Langzeituntersuchung Bei Einem Vollkeramik Kronensystem (Cerestore', thesis)," Zurich: University of Zurich. Malament, K.A. (1987). "The Cast Glass-Ceramic Restoration". Journal of Prosthetic Dentistry, Vol. 57, 1989, pp. 674-683.
36. Thompson, J.Y., Anusavice, K.J., Naman, A., and Morris, H.F., "Fracture Surface Characterization of Clinically Failed All-Ceramic Crowns," Journal of Dental Research, Vol. 73, No. 12, 1994, pp. 1824-1832.
37. Kelly, J.R., Tesk, J.A., and Sorensen, J.A., "Failure of All-Ceramic Fixed Partial Dentures In Vitro and In Vivo: Analysis and Modeling," Journal of Dental Research, Vol. 74, No. 6, 1995, pp. 1253-1258.
38. Anusavice, K.J., and Hojjatie, B., "Tensile Stress in Glass-Ceramic Crowns: Effect of Flaws and Cement Voids," International Journal of Prosthodont, Vol. 5, 1992, pp. 351-358.
39. Hojjatie, B., "Optimization of the Biaxial Test Conditions by Finite Element Analysis," Journal of Dental Research, abstract no. 1397, 1992, pp. 690.
40. Anusavice, K.J.,ISO 6872 report for Dental Ceramic Round Robin Testing, 1991.
41. Marshall, D.B., "An Improved Biaxial Flexure Test for Ceramics," Ceram Bulletin 59, 1980, pp. 551-553
42. Young, W.C., "Roark's Formulas for Stress & Strain, Sixth Edition," New York, McGraw-Hill Book Company, 1989, p. 432.
43. Ringle, R.D., private conversation, Aug. 26, 1994.
44. Anusavice, K.J., Hojjatie, B., "Influence of Incisal Length of Ceramic and Loading Orientation on Stress Distribution in Ceramic Crowns," Journal of Dental Research, Vol. 67, 1988, pp. 1371-1375
45. Hojjatie, B., Anusavice, K.J., "Three-Dimensional Finite Element Analysis of Glass-Ceramic Dental Crowns," Journal of Biomechanics, Vol. 23, No. 11, 1990, pp. 1157-1166.
46. Wheeler, R.C., A Textbook of Dental Anatomy and Physiology. 4th edn., W.B. Saunders, Philadelphia, 1965, pp. 21..
47. Craig, R.G., "Restorative Dental Materials, Ninth Edition," Mosby-Year Book, Inc., 1993, p. 62.

Table 1: Summary of statistical parameters for the biaxial flexure specimens.

	PORCELAIN B		PORCELAIN O	
	Surface	Volume	Surface	Volume
σ_θ (MPa•mm$^{3/m}$)	67.6	57.6	100	83.9
σ_θ (MPa)	70.2	70.2	102	102
m	15.7	15.7	14.0	14.0
A_s (mm^2)	167	N/A	167	N/A
V_s (mm^3)	N/A	133	N/A	133

Table 2: Summary of statistical parameters for the biaxial flexure specimens

	PORCELAIN B		PORCELAIN C1/C3	
	Surface	Volume	Surface	Volume
σ_θ (MPa•mm$^{3/m}$)	73.0	57.5	93.2	72.2
σ_θ (MPa)	78.8	78.8	99.5	99.5
m	15.5	15.5	14.8	14.8
N	25.8	25.8	28.5	28.5
B (MPa^2•sec)	0.06	0.05	0.01	0.008
ln A	3.89	3.89	4.1	4.1
A_s (mm^2)	37.5	N/A	37.5	N/A
V_s (mm^3)	N/A	82.5	N/A	82.5

Table 3: Probability of failure and maximum stress for each group of elements within the porcelain. Element groups are listed by material type and (material number).

300 NEWTON LOAD PERPENDICULAR TO SURFACE			
Material Type(#)	Fracture Origin	P_f	σ_f (MPa)
B(1)	Volume	0.1146E-01	70
O(2)	Volume	0.6416E-06	50
B(5)	Surface	0.3232E-07	26
O(6)	Surface	0.3453E-13	12
B(7)	Surface	0.4219E-14	9
O(8)	Surface	0.0000E+00	6
O(9)	Surface	0.4996E-14	10
Overall Volume P_f	0.1146E-01		
Overall Surface P_f	0.3232E-07		

300 NEWTON LOAD 30° FROM PERPENDICULAR LOAD CASE			
Material Type(#)	Fracture Origin	P_f	σ_f (MPa)
B(1)	Volume	0.1194E+00	81
O(2)	Volume	0.4516E-06	50
B(5)	Surface	0.5865E-07	27
O(6)	Surface	0.0000E+00	9
B(7)	Surface	0.0000E+00	1
O(8)	Surface	0.0000E+00	0.2
O(9)	Surface	0.0000E+00	2
Overall Volume P_f	0.1194E+00		
Overall Surface P_f	0.5865E-07		

600 NEWTON LOAD APPLIED VERTICAL TO CROWN			
Material Type(#)	Fracture Origin	P_f	σ_f (MPa)
B(1)	Volume	0.3552E+00	91
O(2)	Volume	0.3897E-03	83
B(5)	Surface	0.8173E-11	15
O(6)	Surface	0.1060E-10	17
B(7)	Surface	0.0000E+00	7
O(8)	Surface	0.0000E+00	4
O(9)	Surface	0.0000E+00	6
Overall Volume P_f	0.3555E+00		
Overall Surface P_f	0.1877E-10		

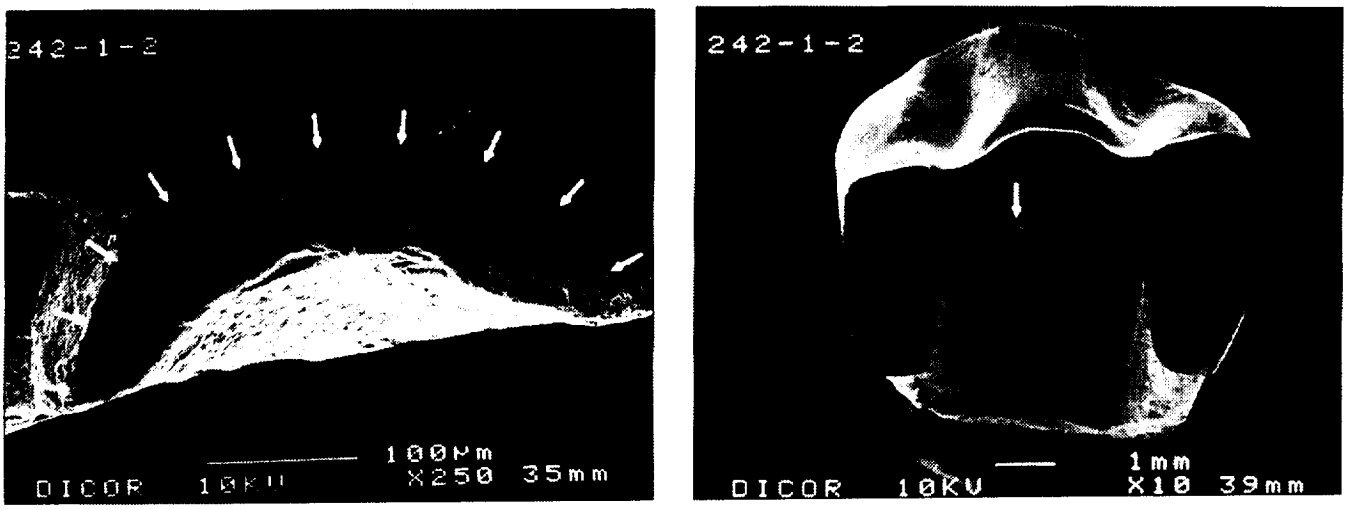

Figure 1.—Fractographic results of an all Dicor® crown showing failure initation along the internal surface of the crown. Figure taken from reference 36.

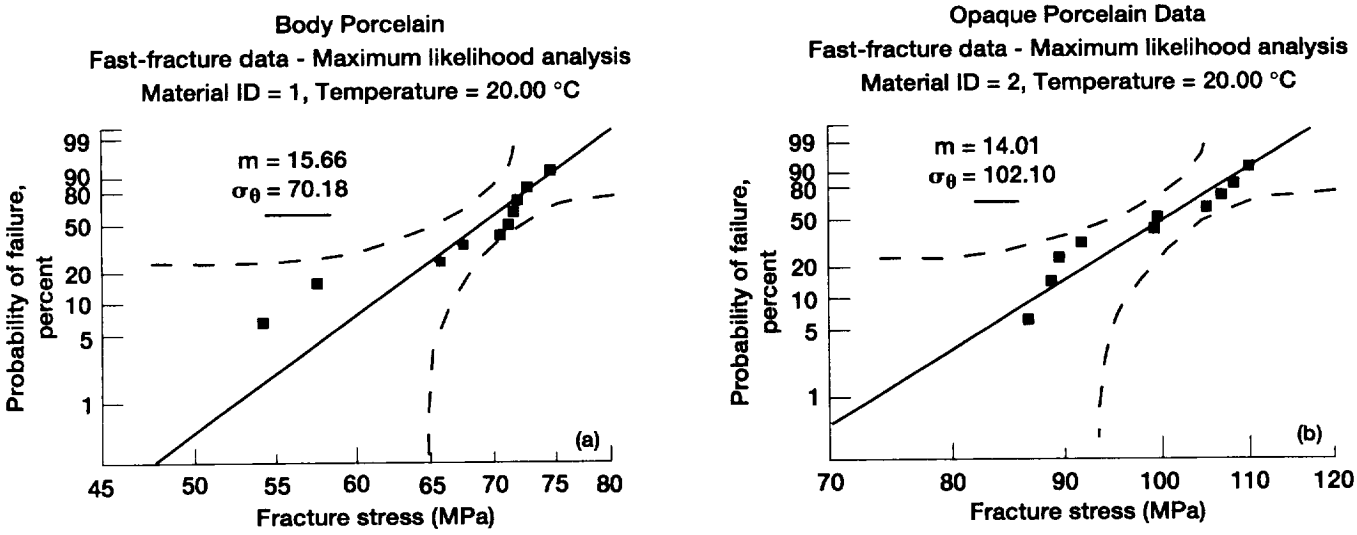

Figure 2.—Weibull plot of (a) body porcelain and (b) opaque porcelain fast-fracture data reproduced (39) and (40). Dotted lines represent Kanofsky-Srinivasan 90 percent confidence bands.

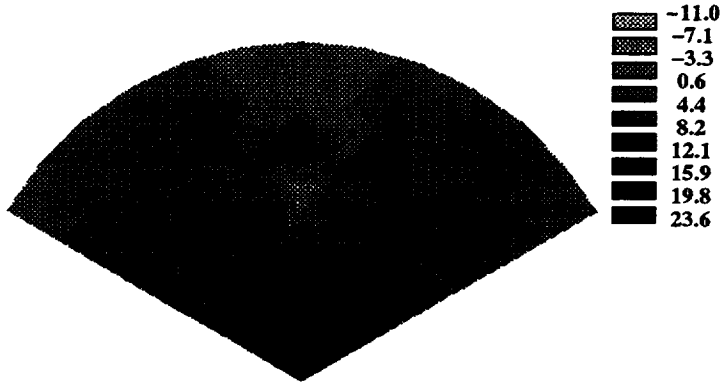

Figure 3.—ANSYS® Plot of the principal stress on a biaxial test specimen. This model was used to analyze data from reference 40.

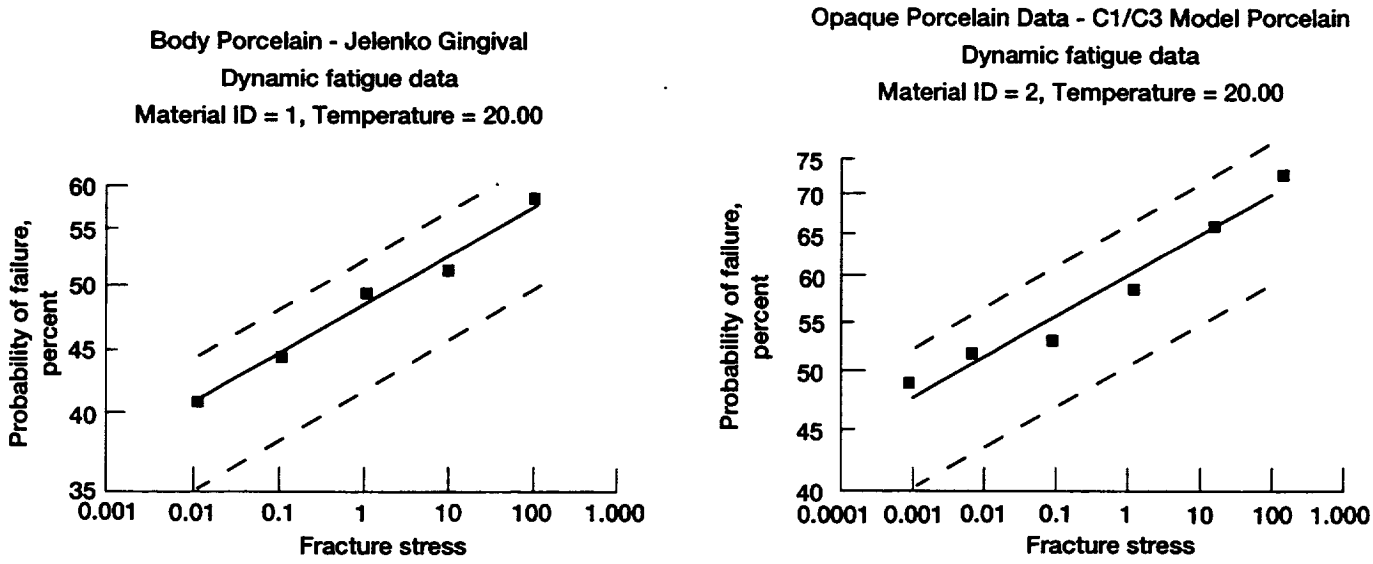

Figure 4.—Plot of median data values at various stressing rates (dynamic fatigue) of (a) body porcelain and (b) C1/C3 model porcelain taken from reference 28. Dotted lines represent 90 percent scatter band of the individual rupture stresses.

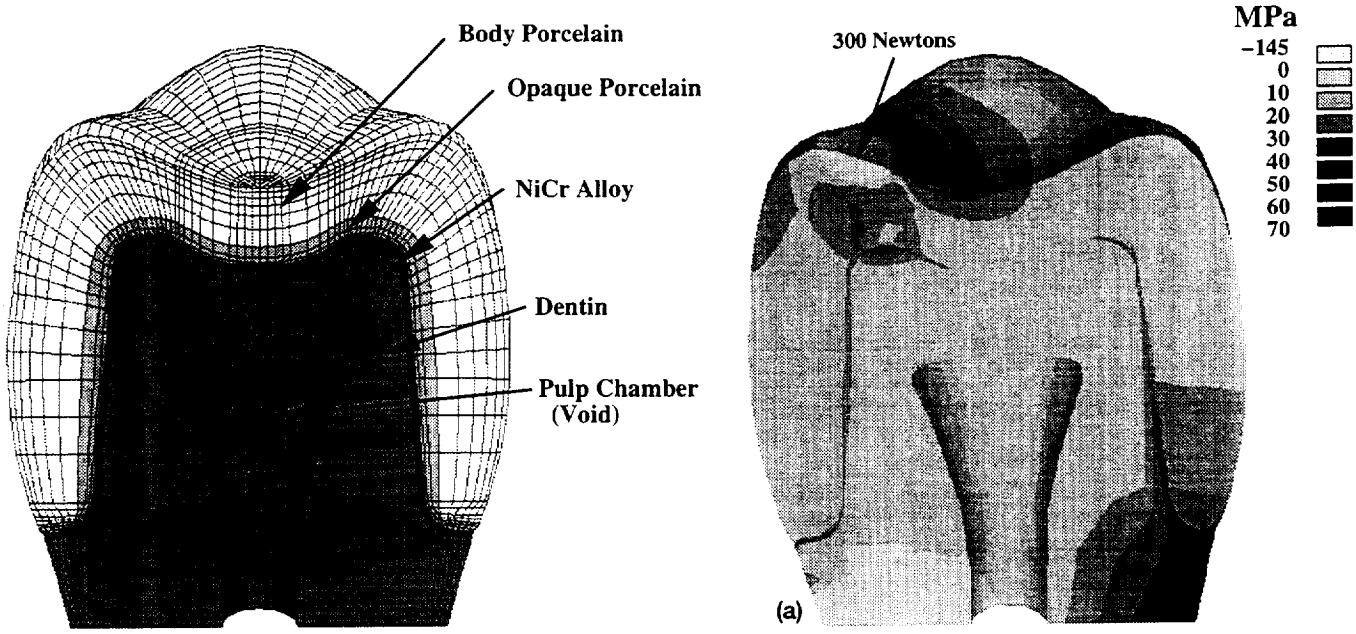

Figure 5.—Cutting plane view of three dimensional PFM molar crown used for this analysis. (Top of model is titled in 30°).

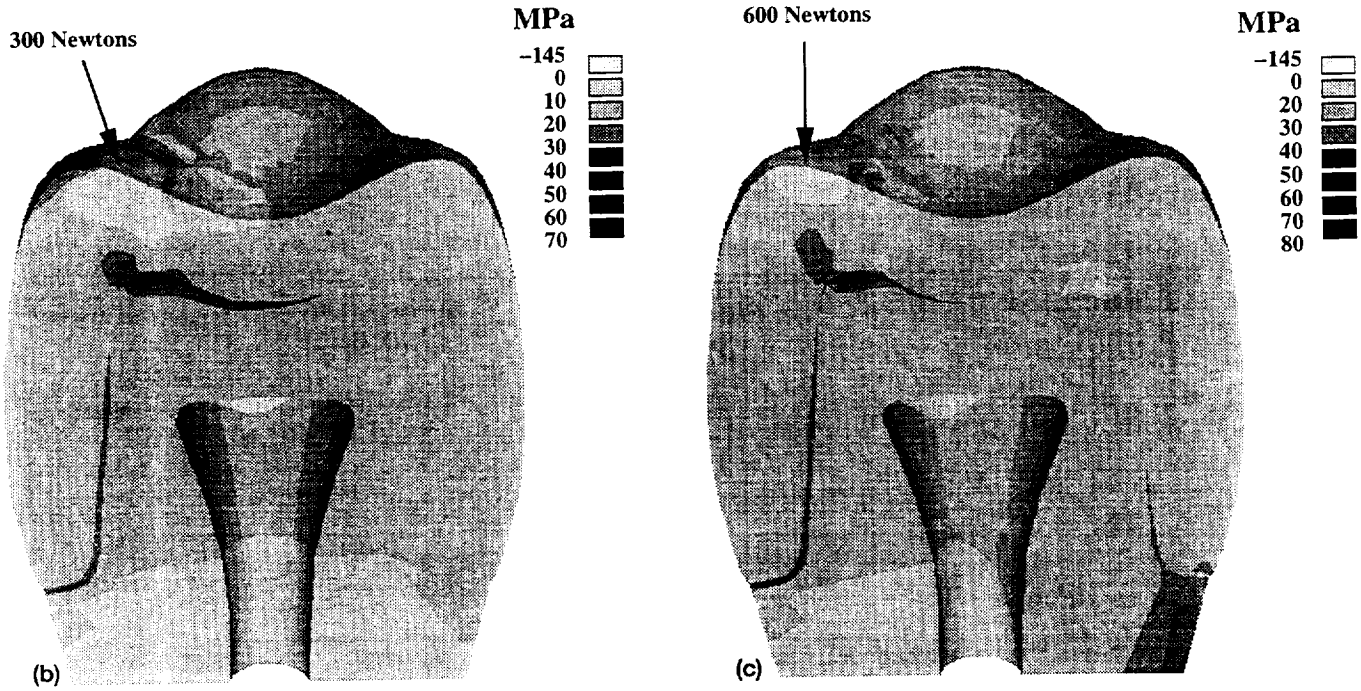

Figure 6.—(a) First principle stress plot for load case perpendicular to surface. (b) First principle stress plot for load case 30° from perpendicular to surface. (c) First principle stress plot for vertical loadcase.

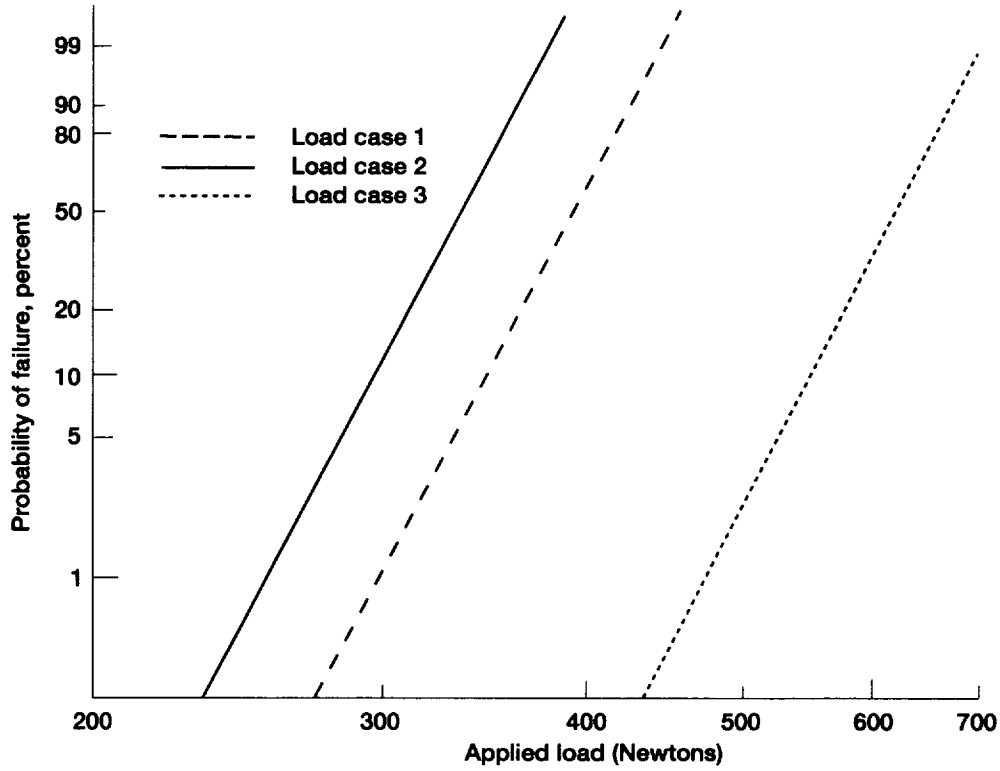

Figure 7.—Weibull plot of fast-fracture failure probability versus applied load for each load case for (a)

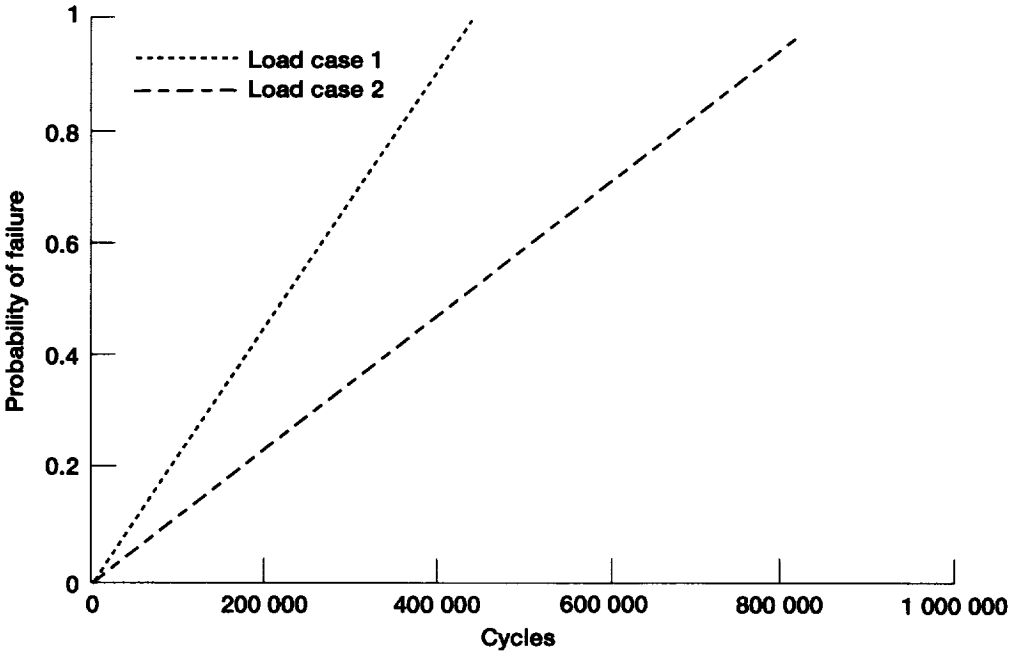

Figure 8.—Cycle dependent probability of failure for surface flaws on exposed surface of body 1 porcelain. Highest failure rates correspond to the perpendicular load case (Load case 1). Followed by the 30 degrees from perpendicular load case (Load case 2).

REPORT DOCUMENTATION PAGE

Form Approved
OMB No. 0704-0188

1. AGENCY USE ONLY (*Leave blank*)	2. REPORT DATE	3. REPORT TYPE AND DATES COVERED
	March 1996	Technical Memorandum

4. TITLE AND SUBTITLE

Stress and Reliability Analysis of a Metal-Ceramic Dental Crown

5. FUNDING NUMBERS

WU-505-63-5B

6. AUTHOR(S)

Todd M. Sokolowski, Barry Hojjatie, Noel N. Nemeth,
and Kenneth J. Anusavice

7. PERFORMING ORGANIZATION NAME(S) AND ADDRESS(ES)

National Aeronautics and Space Administration
Lewis Research Center
Cleveland, Ohio 44135-3191

8. PERFORMING ORGANIZATION REPORT NUMBER

E-10141

9. SPONSORING/MONITORING AGENCY NAME(S) AND ADDRESS(ES)

National Aeronautics and Space Administration
Washington, D.C. 20546-0001

10. SPONSORING/MONITORING AGENCY REPORT NUMBER

NASA TM-107178

11. SUPPLEMENTARY NOTES

Prepared for the ANSYS Conference and Exhibition, sponsored by ANSYS, Inc., Pittsburgh, Pennsylvania, May 20–22, 1996. Todd M. Sokolowski, The Ohio State University, Department of Mechanical Engineering, Columbus, Ohio; Barry Hojjatie and Kenneth J. Anusavice, University of Florida, College of Dentistry, Gainesville, Florida; and Noel N. Nemeth, NASA Lewis Research Center. Responsible person, Noel N. Nemeth, organization code 5250, (216) 433-3215.

12a. DISTRIBUTION/AVAILABILITY STATEMENT

Unclassified - Unlimited
Subject Category 54

This publication is available from the NASA Center for Aerospace Information, (301) 621-0390.

12b. DISTRIBUTION CODE

13. ABSTRACT ***(Maximum 200 words)***

Interaction of mechanical and thermal stresses with the flaws and microcracks within the ceramic region of metal-ceramic dental crowns can result in catastrophic or delayed failure of these restorations. The objective of this study was to determine the combined influence of induced functional stresses and pre-existing flaws and microcracks on the time-dependent probability of failure of a metal-ceramic molar crown. A three-dimensional finite element model of a porcelain-fused-to-metal (PFM) molar crown was developed using the ANSYS® finite element program. The crown consisted of a body porcelain, opaque porcelain, and a metal substrate. The model had a 300 Newton load applied perpendicular to one cusp, a load of 300N applied at 30 degrees from the perpendicular load case, directed toward the center, and a 600 Newton vertical load. Ceramic specimens were subjected to a biaxial flexure test and the load-to-failure of each specimen was measured. The results of the finite element stress analysis and the flexure tests were incorporated in the NASA developed CARES/LIFE program to determine the Weibull and fatigue parameters and time-dependent fracture reliability of the PFM crown. CARES/LIFE calculates the time-dependent reliability of monolithic ceramic components subjected to thermomechanical and/or proof test loading. This program is an extension of the CARES (Ceramics Analysis and Reliability Evaluation of Structures) computer program.

14. SUBJECT TERMS

Ceramics; Reliability; Weibull; Batdorf; Dental crown; Molar

15. NUMBER OF PAGES

20

16. PRICE CODE

A03

17. SECURITY CLASSIFICATION OF REPORT	18. SECURITY CLASSIFICATION OF THIS PAGE	19. SECURITY CLASSIFICATION OF ABSTRACT	20. LIMITATION OF ABSTRACT
Unclassified	Unclassified	Unclassified	

National Aeronautics and
Space Administration

Lewis Research Center
21000 Brookpark Rd.
Cleveland, OH 44135-3191